Energy ***65*** *(2014) 612-620.*

http://dx.doi.org/10.1016/j.energy.2013.11.067

Enhanced performance of a silicon microfabricated direct methanol fuel cell with PtRu catalysts supported on few-walled carbon nanotubes

Maryam Borghei[a*], Gianmario Scotti[b], Petri Kanninen[c], Timo Weckman[c], Ilya V. Anoshkin[a], Albert G. Nasibulin[a], Sami Franssila[b], Esko I. Kauppinen[a], Tanja Kallio[c], Virginia Ruiz[d]

[a]Department of Applied Physics, Aalto University, P.O. Box 15100, FI-00076 AALTO, Finland

[b]Department of Materials Science & Engineering, P.O.B. 16200, FI-00076 Aalto, Finland

[c]Department of Chemistry, Aalto University, Helsinki, P.O. Box 16100, FI-00076 AALTO, Finland

[d]IK4-CIDETEC -Centre for Electrochemical Technologies, Paseo Miramón 196, E-20009 Donostia-San Sebastián, Spain

*Corresponding author: Tel.: +358 503608519; Fax: +358 947023517; E-mail address: maryam.borghei@aalto.fi.

Abstract

Silicon micro fuel cells (Si-MFCs) are promising power supplies for microelectronic applications, however their development is still at early stages compared to the conventional proton exchange membrane fuel cells (PEMFCs). There are not many published reports on the durability of Si-MFCs and those available only projected the life-time of standard Vulcan based catalysts. However, the limited durability resulting from carbon corrosion is one of the crucial issues in fuel cells. In this study, Si-MFC with an integrated silicon nanograss diffusion layer is used for the direct methanol fuel cell investigations. The long-term (3-day) performance of PtRu catalysts supported on different

carbon supports, namely Vulcan, Graphitized carbon nanofibers (GNFs) and Few-walled carbon nanotubes (FWCNTs), was studied. PtRu-FWCNTs and PtRu-GNFs exhibited respectively 471% (20.0 mW cm^{-2}) and 274% (13.1 mW cm^{-2}) power density enhancements compared to PtRu-Vulcan (3.5 mW cm^{-2}). After 3-day durability measurements, power density stayed at 72, 68 and 91% of the initial value, respectively for PtRu-FWCNTs, PtRu-GNFs and PtRu-Vulcan. To evaluate the influence of carbon supports as well as the distribution and the size of the nanoparticles on the overall performance of Si-MFCs, further characterizations with Raman, BET, XRD, SEM and TEM were performed.

Keywords

Silicon micro fuel cell; Durability; Direct Methanol; PtRu-catalysts; Carbon nanotubes

1. Introduction

The rise of portable electronic devices such as mobile phones, digital cameras and portable computers brings to the fore the crucial issue of power supplies. Down-scaled fuel cells can be applied as a long-lasting, low-cost and eco-friendly miniature energy source as the microelectronic industry develops. The micro fuel cell (MFC) approach is significantly influenced by two technology choices: the nature of the fuel to be used at the anode (i.e. hydrogen or an alcohol), and the fuel cell architecture. Direct methanol micro fuel cells (DM-MFC) are more attractive candidates for portable electronic devices, military radio systems and implantable medical tools. They offer several advantages such as light weight, cheap liquid fuel, easy handling and fast recharging. DM-MFCs can also be operated at ambient temperature and provide almost 10-times higher power density than existing Li-ion rechargeable batteries [1-6].

The catalyst layer is also an important factor, which considerably influences the fuel cell performance. In the case of methanol oxidation, the state-of-the-art anode catalyst is bimetallic platinum-ruthenium on a carbon support, commonly carbon black. However, catalysts are susceptible to degradation under fuel cell conditions because of carbon corrosion, Pt aggregation and Ru dissolution [7]. Therefore, with the aim of enhancing activity and stability of direct methanol fuel cell (DMFC) electrodes, different carbon supports have been investigated such as single-walled (SW-) and multiwalled (MW-) carbon nanotubes (CNTs), graphene, carbon nanofibers (CNFs), fullerenes, carbon nanohorns and mesoporous carbon [8-12]. Specifically CNTs [13-15] and CNFs [16-18] have been studied as catalysts supports because of their outstanding conductivity, thermal and mechanical stability [19]. Their performance has also been compared with each other [20-22].

Liu et al. [13] studied SWCNTs and Vulcan XC-72 supported Pt and PtRu in a DMFC and observed that the SWCNTs-supported catalysts performed better. Similarly, Dillert et al [14] found improved performance with oxidized SWCNTs as support material. On the other hand, Cui et al [15] showed that PtRu supported on MWCNTs provide 33% better power density than a commercial catalyst. Guo et al. [16] studied herringbone-CNFs in oxidized and reduced form; both outperforming Vulcan supported catalyst by 10% in maximum power density. Tsuji et al [17] deposited PtRu on three different types of CNFs (platelet, herringbone and tubular). They concluded that the electrocatalytic activity of CNFs was 70-200% higher than that of a commercial carbon black support. Kang et al. [18] studied the long-term stability of PtRu-CNFs in a DMFC for 2000 h and found that the voltage decay rate was about 60% of the commercial Vulcan catalyst. In addition, metal dissolution rate was 40-70% smaller, although the DMFC performance was almost similar.

Direct comparison between different carbon supports resulted in conflicting reports. Steigerwalt et al. [20] studied various supports and reported that only herringbone-CNFs could improve DMFC

performance compared to unsupported PtRu catalyst. PtRu-SWCNTs and PtRu-MWCNTs performed better than other types of CNFs but worse than unsupported PtRu. Girishkumar et al [21] studied SWCNTs from several manufacturers, MWCNTs, CNFs and carbon black as support materials. All the alternative supports outperformed carbon black both in a 3-electrode half-cell and in a DMFC in the order of SWCNTs > MWCNTs > CNFs > carbon black. However, they found large differences in performance between various SWCNTs and indicated that catalytic properties are not only dependent on the general type of carbon support but also on the exact properties of the individual carbon material.

MFC technology is still relatively young compared to the more established PEMFC. To the best of our knowledge, there are not many published reports on the durability of Si-MFCs and those available only projected the life-time of standard Vulcan based catalysts. Jiang et al. [22] studied short-term performance of their direct methanol micro fuel cell with a commercial E-Tek catalyst (60 wt% PtRu-Vulcan) only for 2 h. Since the first report on miniature methanol fuel cell with silicon substrates [23], most of the MFC development was done using microfabrication technologies, and the MFC performance was investigated only with the standard carbon black based catalyst [3, 24].

The objective of this work is to enhance the performance of our Si-MFCs with catalyst materials other than the standard supported Vulcan catalyst in order to evaluate the influence of electrode structure and fuel cell architecture on the activity and long-term durability. Electrode material evaluation at the micro scale requires less amount of catalyst material than a macro scale fuel cell. Moreover, preparation of membrane electrode assembly (MEA) is also less time consuming due to the smaller area of the cell. Hence, we propose that the down-scaled MFC could be used as a fast and material sparing tool for catalyst performance assessment, prior to applying large amounts of novel materials in large scale fuel cells. Previously, we studied methanol oxidation using PtRu-catalysts supported on FWCNTs, GNFs and Vulcan, both in a half-cell and a DMFC, the latter with

a cell area of 7.29 cm^2 [25]. It was concluded that 6-day DMFC durability tests were different from one hour half-cell stability experiments. It was found that half-cell measurements cannot be necessarily comparable to fuel cell results because of many parameters affecting fuel cell performance. In this study, we have examined several catalyst materials in a different type of fuel cell and under different operation conditions. Specially, Si-MFC with the cell area of 1 cm^2 was prepared from highly boron-doped silicon wafer and silicon nanograss was fabricated on top of the flow fields as integrated diffusion layer (DL). PtRu nanoparticles were deposited on FWCNTs, GNFs and the Vulcan supports by a polyol method and characterized by different techniques. Performance and durability of catalysts in Si-MFCs were investigated by chronoamperometric (CA) measurements for three days (72 h).

2. Experimental

2.1. Carbon supports and catalysis synthesis

FWCNTs were synthesized via decomposition of CH_4 diluted with H_2 at 950 °C on CoMo-MgO catalyst [26]. GNFs were kindly supplied by Showa Denko (Japan). Vulcan XC-72, powdered carbon black was purchased from Cabot Corporation. In order to create active sites to anchor metal particles, oxidative surface functionalization was performed in a refluxing condition with 2 M HNO_3/1 M H_2SO_4 (1:1) at 120 °C both on GNFs for 6 h and FWCNTs for 4h. PtRu catalysts (total loading of 30 wt%, Pt:Ru 1:1 atomic ratio) were deposited on the carbon supports by a polyol method. The required amount of metal precursors, K_2PtCl_4 and $RuCl_3$, were mixed with ethylene glycol and water. The metal suspension was added to the carbon support and 0.4M NaOH/0.04M $NaBH_4$ solution was added dropwise under vigorous agitation. The resulting suspension kept in ultrasound bath for 2 h at 60 °C. Lastly, the suspension was filtered, rinsed and dried in vacuum oven over night.

2.2. Physical characterization

Scanning electron microscopy (SEM) was carried out with a field emission JEOL microscope JSM-7500FA equipped with an energy dispersive X-rays spectrometer (EDXS). Transmission Electron microscopy (TEM) was performed using a Tecnai 12 BioTwin with LaB_6 gun at 120 kV. High resolution TEM (HR-TEM) was done with a double Cs-corrected JEOL (JEM-2200FS) combined with a 200 kV field emission gun. X-ray diffraction (XRD) spectra were obtained by a Bruker D8 advanced X-ray diffractometer using Cu-Kα radiation and a Lynx Eye fast detector with scan conditions of 2 s/0.03°. Brunauer-Emmett-Teller (BET) surface area measurements were done by N_2 adsorption-desorption isotherms at 77 K with a FlowSorb 2300II instrument by Micromeritics. Raman analysis was performed using a Horiba LabRAM HR spectrometer equipped with CCD camera and a 633 nm laser beam.

2.3. Microfabrication of the silicon chips

The silicon chips were microfabricated from a highly boron-doped silicon wafer, using a process as shown in Fig. 1. The wafer was thermally oxidized at 1100 °C to form a 500 nm thick layer of SiO_2 and then patterned with photolithography and etching in a HF solution (a) to determine the silicon nanograss area. This was followed by a second photolithography (b) and a reactive ion etching (RIE) to create the flow field (c). A 200 nm thick layer of aluminum was sputtered on the back of the wafer, and patterned with photolithography to create a mask for a through-wafer deep RIE etching (d), opening the inlet holes in the chips. Finally, silicon nanograss was formed over the flow filed by RIE in passivating conditions, and 40 nm of chromium was sputtered on top to improve conductivity and slow down silicon oxidation (e). Silicon nanograss is a quasi-random array of needle-like silicon structures, about 2 μm tall and 200-300 nm wide at the base (shown in the inset

of Fig. 1). It is formed when silicon is etched in reactive plasma under passivating conditions (high ratio of O_2 to SF_6 gas flow at cryogenic temperatures) More details of the process are found in [27].

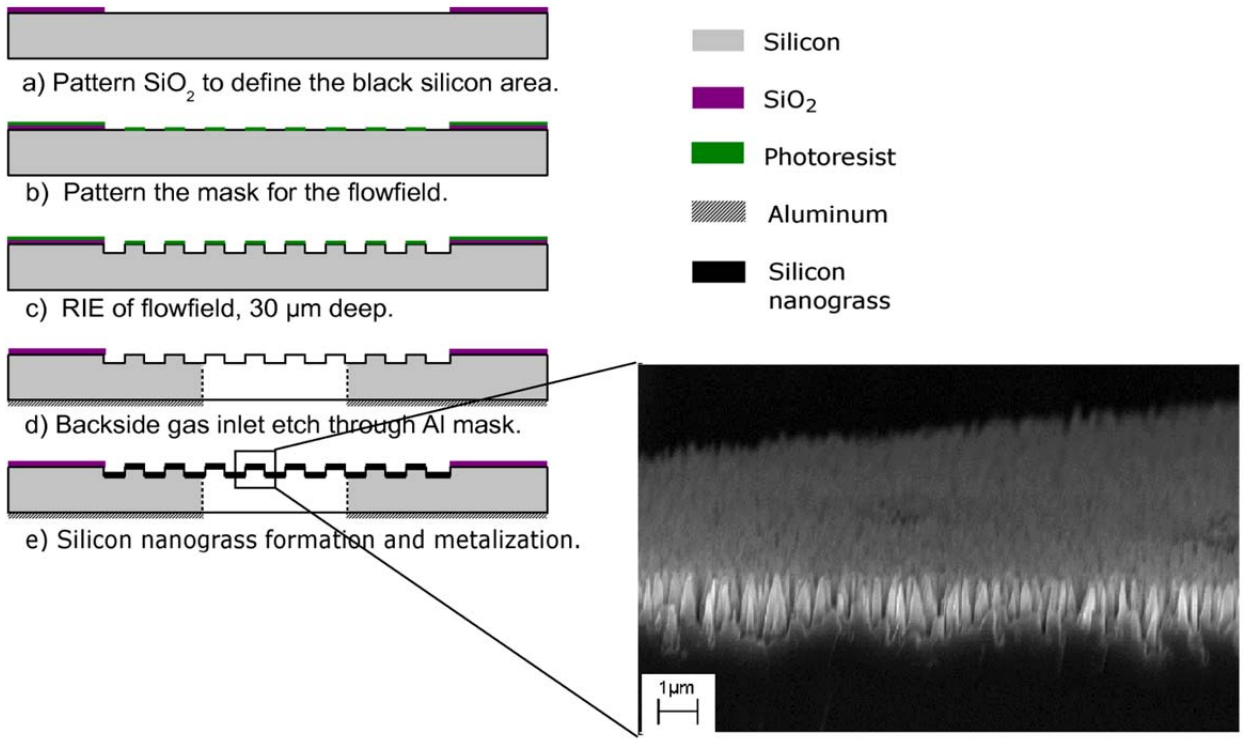

Fig. 1. Main steps of microfabrication of a silicon chip. The inset shows nanograss formed on top of the flow fields.

2.4. Si-MFC measurements

Nafion® 115 was used as the solid electrolyte membrane in the fuel cell and it was cleaned by boiling sequentially in 5 wt% H_2O_2, 0.5 M H_2SO_4 and deionized water. The catalyst ink was prepared by mixing the catalyst, 60 wt% Pt on carbon black (Alfa Aesar) for the cathode and the synthesized PtRu on various supports for the anode, with 5 wt% Nafion dispersion. Isopropanol and water were added to control the viscosity of the ink. The components were mixed by a magnetic stirrer for several hours with additional 30 minutes of sonication. The resulting slurry was painted on the Nafion® membrane by an air brush to prepare MEAs. PtRu loadings for each anode were as follows (in mg cm^{-2}): 0.99 (Vulcan), 0.87 (GNFs) and 0.85 (FWCNTs). Cathode Pt loading was

approximately 2 mg cm^{-2} in each MEA to ensure that it does not limit the performance. Nafion® content of the anode and the cathode were 30 wt% and 20 wt%, respectively. Finally, MEAs were hot pressed at 130 °C with 50 bar pressure for 2 minutes. Fig. 2a shows photograph of a silicon cell with the gas inlet holes that are located diagonally. Si-MFC was constructed by sandwiching MEA between the two silicon chips (Fig. 2b).

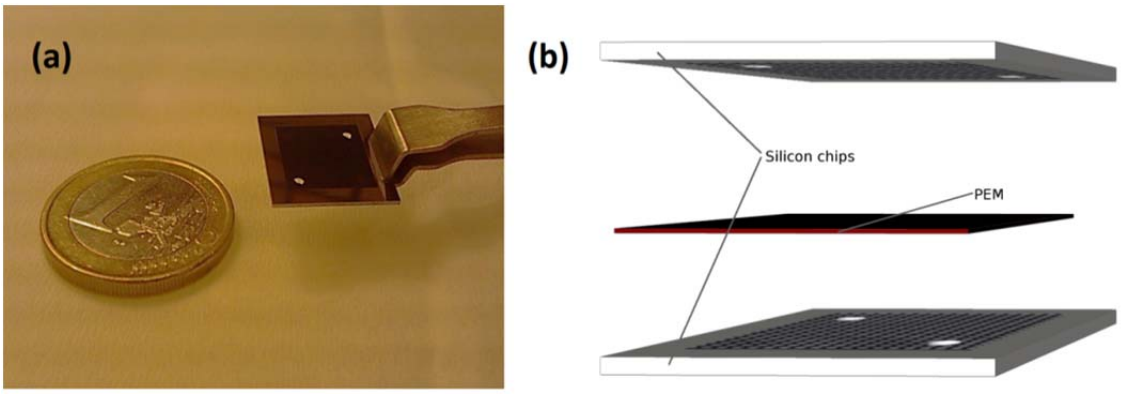

Fig. 2. Photograph of a silicon chip (a) and Si-MFC construction by sandwiching the MEA between two silicon chips (b).

The Si-MFCs were fed with a 1 M methanol solution in deionized water at rate of 0.2 ml min^{-1} to the anode and 50 ml min^{-1} dry O_2 to the cathode. The temperature of the cell was held at 30 °C. Prior to the measurement, the cell was stabilized for 2 hours at 30 °C. Then, a polarization curve was obtained with a voltage sweep from the open circuit voltage (OCV) to 0.1 V at a scan rate of 0.5 mV s^{-1}.

CA stability measurements were carried out at 0.2 V for 72 h, followed by another polarization curve measurement. Fuel cell tests were analysed with a Metrohm Autolab PGSTAT100 potentiostat.

Contact angle measurements on MEAs were made using a KSV Instruments CAM200 optical tensiometer. To eliminate distorting effect of water on dry Nafion [28] and to ensure a completely wetted catalyst layer, MEAs were first boiled in DI water before the contact angle measurements.

Cooled MEAs were removed from water, patted dried on the surface and a static contact angle measurement was made immediately. The contact angle was repeated at least at two locations on MEAs to obtain an average value.

3. Results and Discussions

3.1. Characterization of carbon supports

Morphology of carbon support materials was observed by TEM (Fig. 3). Brunauer-Emmett-Teller (BET) surface area is also reported in Table 1. Vulcan (Fig. 3a) has a turbostratic structure with a particle size of 30-50 nm and 154 $m^2 g^{-1}$ BET surface area. GNFs (Fig. 3b) with average diameter of 150 nm and 10 µm length have very low surface area (17 $m^2 g^{-1}$) whereas FWCNTs (Fig. 3c) with 2-5 walls up to 6 nm diameter and 1µm length, display an extraordinary 449 $m^2 g^{-1}$ surface area.

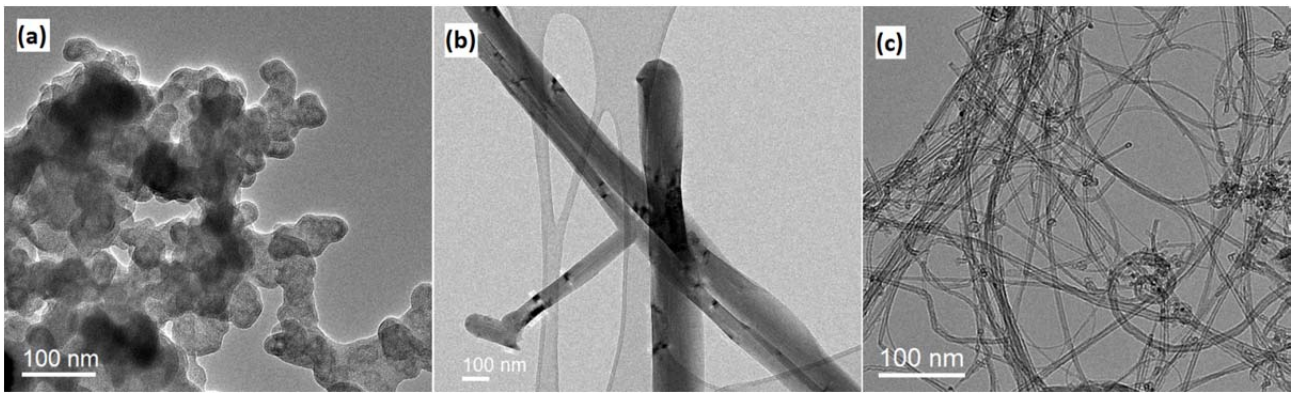

Fig. 3. TEM images of the carbon supports: Vulcan (a), GNFs (b), FWCNTs (c).

Raman spectra of the catalyst supports are shown in Fig. 4. D-band around 1350 cm^{-1} is the characteristic mode for defective structures, and G-band around 1580 cm^{-1} corresponds to graphitic layers [29]. The intensity ratio of D- to G-band (I_D/I_G) for GNFs (0.37) and FWNTs (0.43) shows that both have a highly ordered structure compared to Vulcan (1.2). Pristine GNFs have been subject to a high temperature annealing process (~ 2800 °C), resulting in a high degree of graphitization and very low D- to G-band ratio. The peak shoulder on G-band at 1620 cm^{-1} (D´-

band) occurred from the vacuum annealing at high temperature [30]. A little higher I_D/I_G for FWCNTs together with the broader G-band indicates that nanotubes are in different stages of graphitization. Therefore, in order to produce enough active sites to anchor nanoparticles, longer oxidation treatment was carried out for GNFs than for FWCNTs.

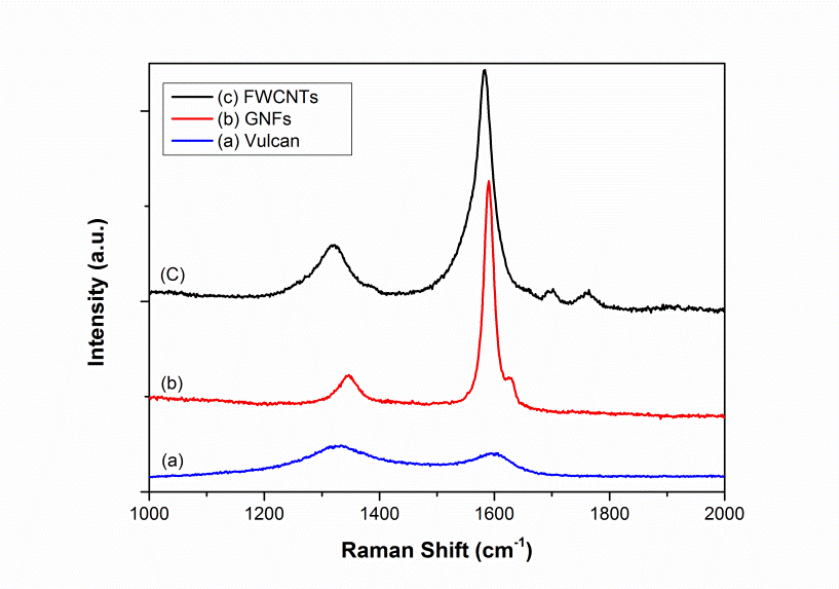

Fig. 4. Raman spectra of pristine Vulcan, GNFs and FWNTs.

3.2. Characterization of PtRu-catalyst powders

The average metal loading and the Pt:Ru ratios were determined by EDXS analysis (Table 1).

A similar catalyst loading was obtained for the three samples even though the carbon supports were different in surface area, morphology and graphitic structure. However, a slight decreasing trend with BET surface area of the carbon supports is observed.

Table 1. BET surface area of the carbon supports, metal loadings and Pt:Ru ratio. (Average size of the catalyst particles are given in Table 4.)

Catalysts	BET area of pristine carbon support (m^2/g)	PtRu loading (wt%)	Pt:Ru (mol ratio)
PtRu-Vulcan	154	27.5	1.3 ± 0.05
PtRu-GNF	17	24.8	1.6 ± 0.13
PtRu-FWNTs	449	28.3	1.8 ± 0.11

Pore volume distributions of PtRu catalysts on Vulcan and FWCNTs are shown in Fig. 5. For PtRu-Vulcan, total pore volume is 0.31 ml g^{-1} with a narrow pore volume distribution centered around 10-20 nm. However, a broader pore size distribution was obtained for PtRu-FWCNTs with a mean size of 4-5 nm and 0.64 ml g^{-1} total pore volume. Unfortunately, pore volume distribution of PtRu-GNFs was not obtained even after several trials probably due to very low BET area of GNF support. For SWCNTs (BET of 400-900 m^2 g^{-1}) a microporous structure has been usually observed by N_2-adsorption whereas for MWCNTs (200-400 m^2 g^{-1}) a mesoporous structure is dominantly obtained [19]. Hence, FWCNTs (449 m^2 g^{-1}) in this study show an intermediate feature between microporous (SWCNTs) and mesoporous (MWCNTs) structures.

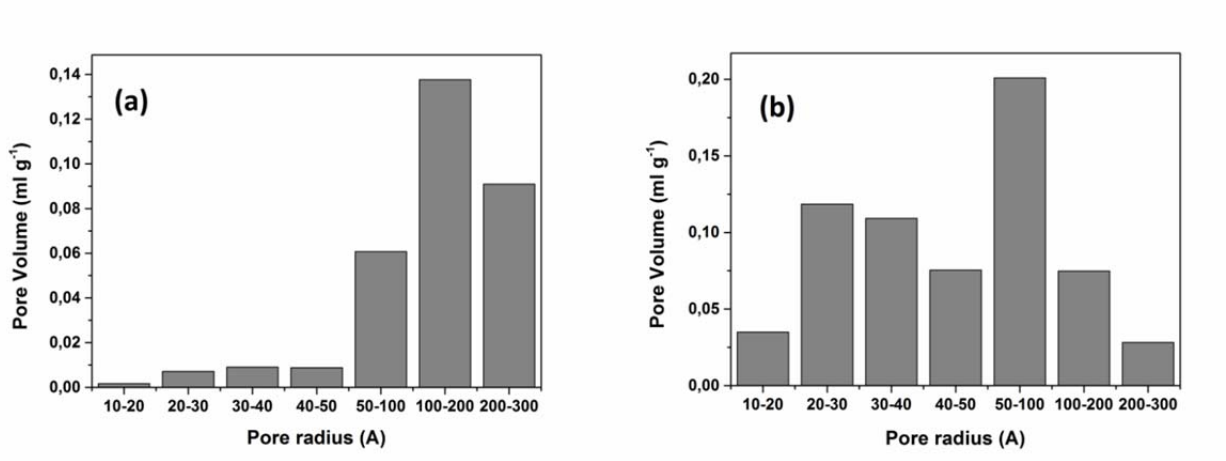

Fig. 5. Pore size distribution of PtRu-Vulcan (a) and PtRu-FWCNTs (b).

3.3. Performance and durability of Si-MFCs

Fig. 6 shows polarization curves (a) and power density measurements (b) before and after 72-h durability experiments. It can be seen that the type of carbon support has a notable effect on the overall fuel cell performance. PtRu-FWCNTs provided the best performance over the whole range of current densities, and displayed the highest maximum power density of 20.0 mW cm^{-2}. PtRu-FWCNTs outperformed by 471% the performance of PtRu-Vulcan (3.5 mW cm^{-2}). This higher power density obtained with PtRu-FWCNTs arises from the unique CNT structure that enhances electron transfer in the electrode. Grishkumar reported [21] significantly lower charge transfer resistance with SWCNTs supported catalysts (~140 Ω) compared to carbon black support (~ 6 kΩ), that resulted in lower onset potential for methanol oxidation and enhanced DMFC performance.

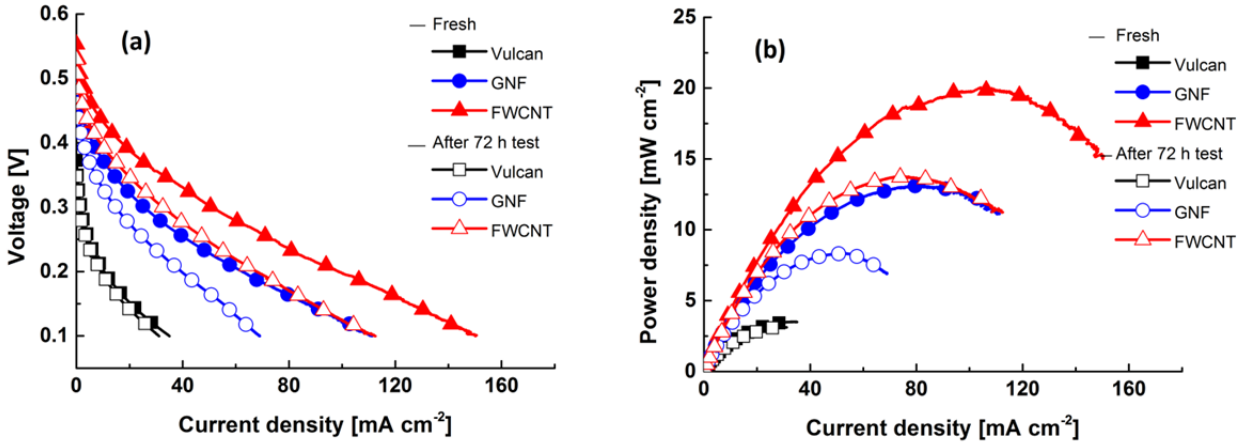

Fig. 6. Polarization curves of current density (a) and power density (b) of PtRu-Vulcan, PtRu-GNFs and PtRu-FWCNTs anodes, before and after the 72 h CA measurements.

PtRu-GNFs (13.1 mW cm^{-2}) outperformed PtRu-Vulcan by 274%. However, the low OCV (0.37 V) and maximum power density (3.5 mW cm^{-2}) for PtRu-Vulcan are in the range of previously published data for Si-MF DMFCs, as listed in Table 2 [23, 31-34]. It is also worthy to mention that PtRu-Vulcan-MEA in this study contains considerably lower metal loading (0.99 mg cm^{-2}) than that reported for MEAs with commercial catalysts (Table 2).

Table 2. Comparison of the performance for Si-MFCs with PtRu-Vulcan anode catalyst.

PtRu, loading in the anode (mg cm^{-2})	Pt, loading in the cathode (mg cm^{-2})	Methanol, (ml min^{-1})	Oxidant(ml min^{-1})	PEM	Temp (°C)	OCV V	P_{max} (mW cm^{-2})	Reference
0.99	2	1 M, 0.2	O_2, 50	Nafion 115	30	0.37	3.5	This work
(60 wt%)	(60 wt%)	2 M, 0.2	air-breath	Nafion 117	25	0.47	2.31	[23]
2	1	2 M	--	Nafion 117	25	0.44	2.5	[31]
2	1	2 M	--	modified Nafion 117	25	0.45	4.9	[31]
4	4	2 M	--	Nafion 117	25	0.47	10	[32]
--	--	10 µL	air-breath	--	--	0.7	0.29	[33]
--	--	1 M, 0.283	O_2, 88	Nafion 112	RT	--	14.3	[34]

All the catalysts showed good performance after a 72-h CA measurement at 0.2 V keeping 78%, 68% and 91% of their initial maximum power density for PtRu-FWCNTs, PtRu-GNFs and PtRu-Vulcan, respectively (Fig. 6b).

Fig. 7 shows 72-h long CA measurements at 0.2 V. PtRu-FWCNTs produced the highest initial current density followed by PtRu-GNFs and then PtRu-Vulcan, in agreement with the trend seen in the polarization curves (Fig. 6a): PtRu –FWCNTs > PtRu-GNFs > PtRu-Vulcan. There is a decrease in performance over time for both PtRu-GNFs and PtRu-FWCNTs. However the current density after three days is still considerably higher for PtRu-FWCNTs (49 mA cm^{-2}) compared to PtRu-GNFs (21 mA cm^{-2}) and PtRu-Vulcan (12 mA cm^{-2}) by 130% and 300% respectively. PtRu-Vulcan showed the lowest current density but the least instability, which could be partly attributed to our experience in MEA preparation and optimization with this standard catalyst material.

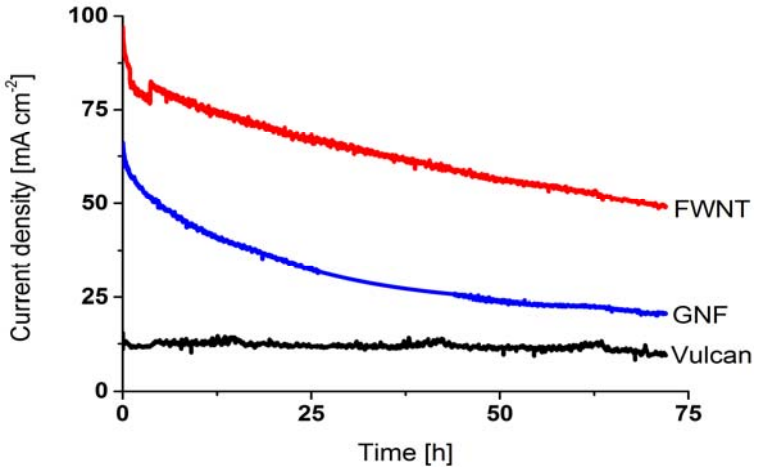

Fig. 7. CA measurements in Si-MFCs with PtRu anode catalysts supported on Vulcan, GNFs and FWCNTs for 72 h at 0.2V.

CA results in Si-MFCs of this work are in agreement with our previous data from half-cell measurements (in 0.1 M $HClO_4$ and 1 M methanol aqueous electrolyte) using PtRu supported FWCNTs, GNFs and Vulcan, where the same order of current density in one hour CA measurements was observed: PtRu-FWCNTs > PtRu-GNFs > PtRu-Vulcan [25]. However, in the previous report the 6-day DMFC durability tests (cell area of 7.29 cm^2) were not in agreement with CA data from half-cell experiments. In that case, PtRu-Vulcan showed the highest current density but more instability compared to PtRu-GNFs and PtRu-FWCNTs. Therefore, it can be concluded that a certain catalyst material may not show the same performance in different fuel cells as the different parameters affecting when the cell architecture is varied. As mentioned before, measurements with Si-MFCs in this study were performed at 30 °C whereas the previous DMFC tests were carried out at 70 °C. Obviously, temperature has a remarkable impact on the fuel cell performance. Moreover, long-term CA measurements in this work have been carried out at 0.2 V in order to obtain higher currents than in previous test conducted at 0.4 V. Other factors such as catalyst layer structure, nanoparticle size distribution along the support, the diffusion layer and cell architecture play notable roles in fuel cell performance as we discuss in the next sections.

3.4. Characterization of the catalyst layers

Cross-sectional SEM micrographs of anode layers before and after 3-day fuel cell tests are illustrated in Fig. 8. Electrode thickness has been measured by observing the cross-section at different locations of MEA, both at the center and around the edges; to ensure the uniformity of the electrode layer and provide a representative average value of electrode thickness (Table 3). Apparently, the pore size distribution of catalysts (Fig. 5) is reflected in the electrode layers. PtRu-FWCNTs layer shows a more compact surface with non-uniform pathways (micro- and meso-size) whereas in PtRu-Vulcan layer evenly-sized pathways can be seen. However, larger macroporous voids are clearly observed in the PtRu-GNFs layer. Despite the large difference in the geometry, structure and properties of the carbon supports, uniform layers with similar thickness were achieved for all the anode catalysts. In addition, no severe changes on the secondary structure of anode layers occurred during the Si-MFC tests, in contrast with our previous work [25] where fresh anode layers had different thickness and a 3-fold increase in thickness was noted for PtRu-Vulcan layer after fuel cell test.

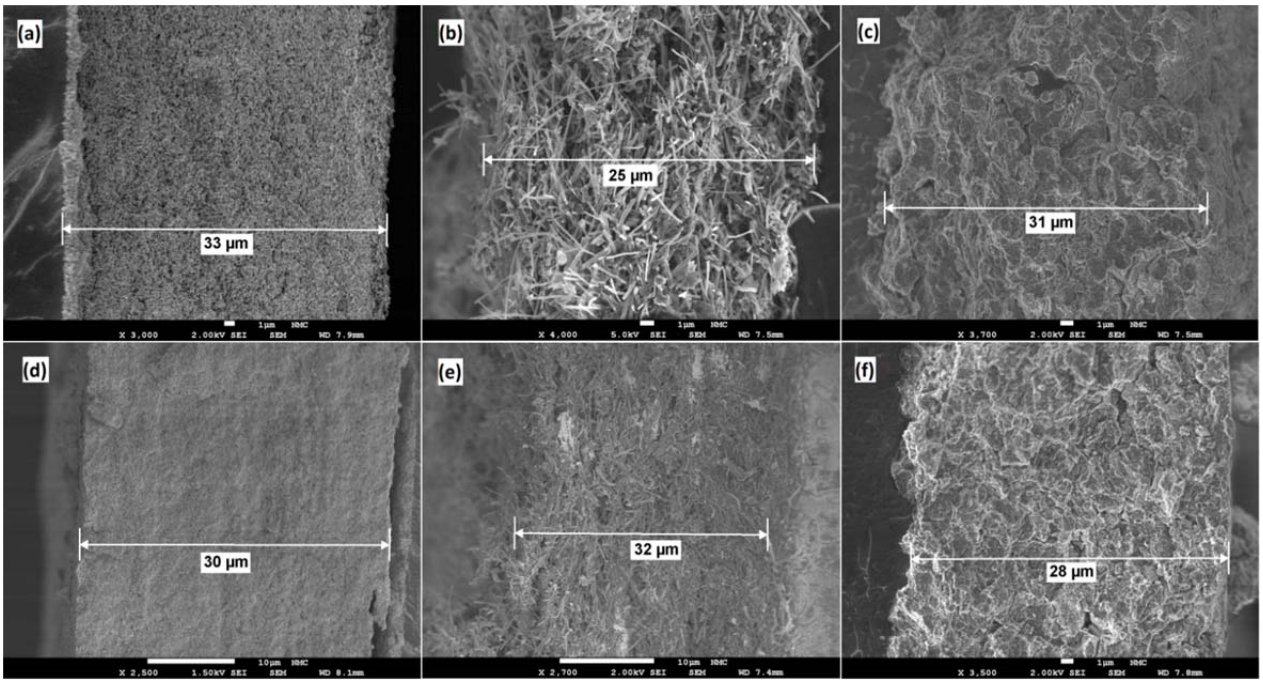

Fig. 8. Cross-sectional SEM images of the anode layers before (a,b,c) and after (d,e,f) the durability tests; with PtRu catalysts on Vulcan (a,d), GNFs (b,e) and FWCNTs (c,f).

Table 3. Average thickness (obtained by SEM images), and contact angle of the anode layers containing PtRu supported on Vulcan, GNFs and FWCNTs before and after the 72-h Si-DMFC tests.

MEA	Average anode thickness (μm)		Contact angle (º)	
	Before	After	Before	After
PtRu-Vulcan	33	30	153	146
PtRu-GNF	25	32	164	156
PtRu-FWNTs	31	28	155	148

Contact angle measurements on fresh and used anode layers have also been performed. Highly hydrophobic catalyst layers with descending order of PtRu-GNFs > PtRu-FWCNTs > PtRu-Vulcan were observed (Table 3). The reason for the slightly higher hydrophobicity of PtRu-GNFs could be highly graphitized walls of GNFs due to annealing at elevated temperatures (lower I_D/I_G in Raman spectra in Fig. 4) together with their elongated geometry that allows the formation of a rough surface with macroscopic gas pockets in the voids (seen in Fig. 8). High hydrophobicity can be beneficial for preventing electrode flooding by liquids in catalyst layers and thus facilitating reactant and product transport. Fuel cell testing leads to a slight decrease of the contact angles (by less than 10º) but all MEAs remain highly hydrophobic even after the measurements.

XRD analysis was carried out from the anode layers of MEAs to measure catalyst particle size before and after durability tests. Fig. 9 shows typical XRD pattern of PtRu-catalysts of the fresh anode layers. The diffraction peaks of PtRu alloy crystal faces (111), (200), (220) and (311) are visible at around 39.9°, 46.3°, 67.8 ° and 81.6° respectively, characteristic of a face-centered cubic (fcc) structure with a cell constant of 3.88 Å for all the catalyst layers [35]. The sharp peaks at 25.1°, 44.3°, 64.6° and 77.7° correspond to Nafion membrane as we previously measured [36]. Hexagonal carbon peak C(002) at around 26.3° is dominant but other characteristic peaks, C(100) at around 42 ° and C(101) at 45°, overlap with PtRu diffraction pattern and consequently are not well

resolved. The average particle size was calculated from PtRu (111) diffraction peak according to Scherrer formula (Table 4). The average PtRu particle size of the fresh catalysts on FWCNTs, GNFs and Vulcan are 2.3, 3.4 and 4.8 nm respectively. After 3-day fuel cell tests, average PtRuparticle size on FWCNTs and GNFs slightly decreased to 2.1 and 3.1 nm, respectively whereas it increased to 5.7 nm for PtRu-Vulcan.

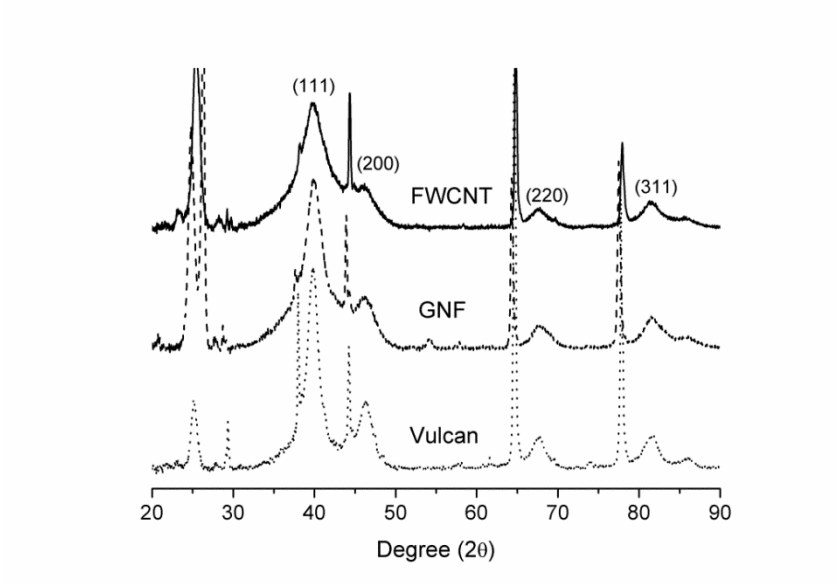

Fig. 9. XRD pattern of the fresh anodes: PtRu supported on Vulcan, GNFs and FWCNTs.

HR-TEM images and corresponding PtRu size distribution histograms of both fresh and used catalysts are depicted in Fig. 10. The mean particle size of all catalysts has been obtained by Gaussian fitting on the histograms (Table 4) showing good agreement with XRD data, except for fresh PtRu-Vulcan MEA. It is probably due to partial blocking of nanoparticles by Nafion® which conceals the smaller particles from X-rays. All the catalysts were well-distributed on the fresh carbon supports but with a narrower distribution on FWCNTs. A broader particle size distribution and more particle aggregates can be observed on the GNF support due to a significantly lower BET surface area and the inertness of GNF walls (originated from high temperature annealing) than that of FWCNTs and Vulcan. Despite good particle distribution and proper size for methanol oxidation on the fresh Vulcan, nanoparticle aggregation was observed after the durability test. This is due to

the corrosion of Vulcan support [37] as well as Ostwald ripening phenomena [38], which result in clustering of the neighboring particles and increase of the particle size distribution. For a Vulcan supported Pt catalyst, Frelink [39] and Joo [40] found that methanol electrooxidation improved with the increase of the particle size from 1.2 to 4.5 nm (when normalized with respect to active platinum sites) whereas for particles beyond 4.5 nm the activity remained almost constant. This is another reason why the activity of our PtRu-Vulcan MEA did not change significantly during the 3-days measurement despite nanoparticle coalescence to around 5.5 nm.

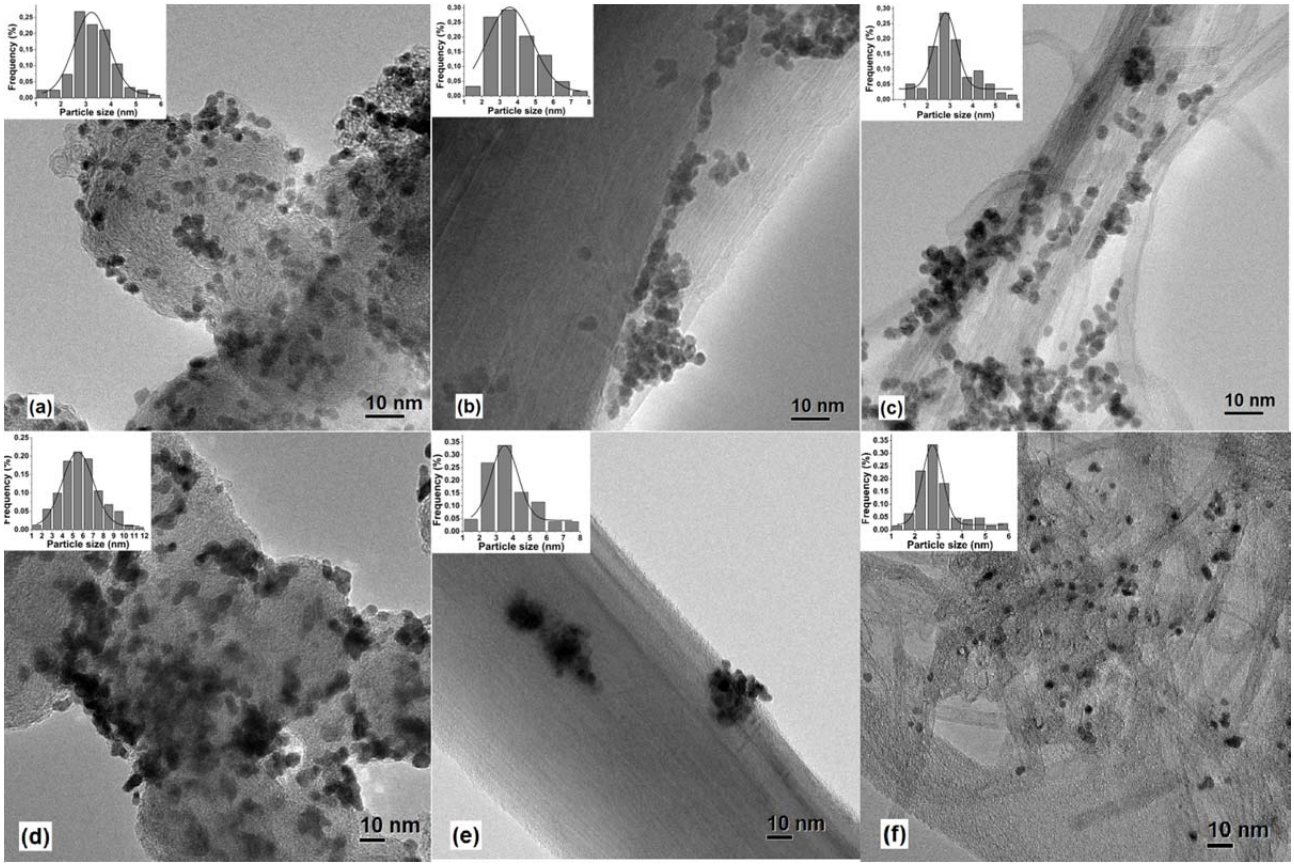

Fig. 10. HR-TEM images and the corresponding PtRu particle size distribution histograms on the fresh supports: Vulcan (a), GNFs (b) and FWCNTs (c), and on the used ones: Vulcan (d), GNFs (e) and FWCNTs (f).

Table 4. Average catalyst size particle from HR-TEM and XRD before and after durability tests.

Catalysts	TEM		XRD	
	Fresh MEA (nm)	Used MEA(nm)	Fresh MEA (nm)	Used MEA (nm)
PtRu-Vulcan	3.6	5.5	4.8	5.7
PtRu-GNF	3.6	3.5	3.4	3.1
PtRu-FWNTs	2.8	2.7	2.3	2.1

Catalyst particles on FWCNTs showed the narrowest size distribution and the smallest average size on the fresh catalyst. The relative number of atoms on the surface is larger for the smaller particles, which results in more electrochemical surface area and electrocatalytic activity. However, the current decrease on PtRu-FWCNTs during 72 h cannot be explained by catalyst aggregation as a narrower particle size distribution and smaller average size was observed on the used catalyst (Fig. 10f). Performance decay could be due to the migration and loss of larger particles from the support to the ionomer which means they became disconnected from the support and did not take part in the electrochemical reaction. Apparently, smaller particles seem to be more strongly attached to the support than larger ones [41]. Therefore, slightly smaller average particle size and distribution was determined for the used PtRu-FWCNTs, both by XRD and HR-TEM (Table 4). In the case of PtRu-GNFs, poor nanoparticle anchoring to the highly inert GNF walls resulted in facile particle detachment from the support (Fig.10e), which can explain the current decrease [42].

We further observed that nanograss tips of DL were partly damaged after the Si-MFC measurements (SEM image not shown). There are two possible phenomena here: one is the mechanical damage of silicon nanograss during fuel cell assembly, the other is corrosion of protective chromium conductive layer. We don't think the latter is significant, and even if it is, it does not lead to silicon shedding. The former does certainly happen, as the silicon element has been detected by EDXS analysis in electrode layers of the used MEAs (with HR-TEM microscope). The

broken silicon debris which was migrated to the catalyst layers may partly clog the pores and hence hinder the efficient mass transport and catalyst access in the MEA.

The type of diffusion layer has also a significant influence on the performance and durability of a fuel cell. In conventional fuel cells, usually a type of carbon cloth or felt is sandwiched between the catalyst layer and the flow field, and its structure controls the catalyst utilization and overall cell performance (in addition to the effect of catalyst material, catalyst layer structure and membrane and flow fields) [43-45]. Water transport and pore filling in all fuel cell layers play important roles in performance [46]. In this study, our Si-MFCs contained silicon nanograss as integrated DL (shown in Fig. 1). While this approach has the advantage of relatively simple fabrication, silicon nanograss length cannot be extended beyond two microns. Such a thin DL may not be enough to provide a uniform flow of reactants to the anode and properly manage water removal from the cathode. Comparing with performances of MEAs, PtRu-FWCNTs produced more than 4-times higher current density than PtRu-Vulcan; consequently more water was formed on the cathode side. Therefore, a gradual coalescence of water droplets may occur in either catalyst layer, DL or flow channels which can increase mass transfer resistance and reduce the overall cell performance [46,47]. In another study [48] a layer of carbon cloth/felt on top of nanograss DL in a H_2/O_2 Si-MFC improved the performance of the cell. Therefore, including an additional layer of mesoporous DL in future studies may not only improve water removal management (at the cathode) and reactant distribution (at the anode) but also prevent migration/loss of catalyst particles from the support, all promoting durability of Si-MFCs.

4. Conclusions

Silicon micro fuel cells (Si-MFCs) were fabricated from highly boron-doped silicon wafer with integrated Si nanograss diffusion layer (DL). Long-term performance of PtRu catalysts on different

carbon supports (GNFs, FWCNTs and Vulcan) was evaluated in direct methanol Si-MFCs at 30 °C for 3 days. PtRu-FWNTs provided the best performance (20.0 $mWcm^{-2}$) followed by PtRu-GNFs (13.1 $mWcm^{-2}$) and PtRu-Vulcan (3.5 $mWcm^{-2}$). However, current decay on PtRu-GNFs and PtRu-FWCNTs was more pronounced than PtRu-Vulcan during durability tests. Catalyst particle size and distribution (HR-TEM and XRD) before and after long-term durability tests showed that catalyst agglomeration was not the reason for the performance decay in the PtRu-FWCNTs. Silicon nanograss may not work efficiently as DL for a uniform distribution of reactant at the anode and water removal at the cathode, which can explain the more pronounced performance decay especially for the most active catalyst (PtRu-FWCNTs) due to the higher water production at the cathode. In addition, the results from Si-MFC tests (in correlation with half-cell measurements of the same catalysts) prove the reliability of the MFC system as a fast and material screening tool for catalysts testing in fuel cell environment.

Acknowledgments

The authors would like to thank Academy of Finland (M.B. and V.R., Academy Research Fellowship), Aalto University (MIDE E.I.K., P.K. and starting grant T.K.), and the Spanish Ministry of Science and Innovation (V.R, Ramón y Cajal Program) for the financial support. This work made use of the Aalto University Nanomicroscopy Center (Aalto-NMC) premises.

References

[1] Yao S, Tang X, Hsieh C, Alyousef Y, Vladimer M, Fedder G et al. Micro-electro-mechanical systems (MEMS)-based micro-scale direct methanol fuel cell development. Energy 2006; 31:636-649.

[2] Yuan Z, Zhang Y, Wenting F, Li Z, Liu W. Investigation of a small-volume direct methanol fuel cell stack for portable applications. Energy 2013; 51: 462-467.

[3] Sundarrajan S, Allakhverdiev SI, Ramakrishna S. Progress and perspective in micro direct methanol fuel cell. Int J Hydrogen Energy 2012; 37:8765-86.

[4] Kamarudin SK, Daud WRW, Ho SL, Hasran UA. Overview on the challenges and developments of micro-direct methanol fuel cells. J Power Sources 2007;163:743-54.

[5] Kundu A, Jang JH, Gil JH, Jung CR, Lee HR, Kim SH, et al. Micro-fuel cells-Current development and applications. J Power Sources 2007;170: 67-78.

[6] Yuan Z, Fu W, Zhao Y, Li Z, Zhang Y, Liu X. Investigation of μDMFC (micro direct methanol fuel cell) with self-adaptive flow rate. Energy 2013;55:1152-8.

[7] Wang ZB, Wang XP, Zuo PJ, Yang BQ, Yin GP, Feng XP. Investigation of the performance decay of anodic PtRu catalyst with working time of direct methanol fuel cells. J Power Sources 2008;181: 93-100.

[8] Antolini E. Carbon supports for low-temperature fuel cell catalysts. App Cat B: Env 2009;88:1-24.

[9] Subhi S, Bruno GP. Support materials for PEMFC and DMFC eletcrocatalysts-A review. J Power Sources 2012;208:96-119.

[10] Lo AY, Hung CT, Yu N, Kuo CT, Liu SB. Synthesis of carbon porous materials with varied pore sizes and their performances as catalyst supports during methanol oxidation reaction. Applied Energy 2012;100:66-74.

[11] Zainoodin AM, Kamarudin SK, Daud WRW. Electrode in direct methanol fuel cells. Int. J Hydrogen Energy 2010;35:4606-21.

[12] Jhan J-Y, Huang Y-W, Teng H, Kuo D, Kuo P-L. Three-dimensional network of graphene grown with carbon nanotubes as carbon support for fuel cells. Energy 2013;53:282-7.

[13] Liu Z, Ling XY, Guo B, Hong L, Lee JY. Pt and PtRu nanoparticles deposited on single-wall carbon nanotubes for methanol electro-oxidation. J Power Sources 2007;167:272-80.

[14] Dillert JF, Bueb H, Dittmeyer R, Weglikowska UD, Roth S. Efficient SWCNT-based anode for DMFC applications. J Electrochem soc 2009;156(10):F137-F144.

[15] Cui Z, Liu C, Liao J, Wei X. Highly active PtRu catalysts supported on carbon nanotubes prepared by modified impregnation method for methanol electro-oxidation. Electrochim Acta 2008;53:7807-11.

[16] Guo J, Sun G, Wang Q, Wang G, Zhou Z, Tang S, et al. Carbon nanofibers supported Pt-Ru eletcrocatalysts for direct methanol fuel cells. Carbon 2006;44:152-7.

[17] Tsuji M, Kubokawa M, Yano R, Miyamae N, Tsuji T, Jun MS, et al. Fast preparation of PtRu catalysts supported on carbon nanofibers by microwave-polyol method and their application to fuel cells. Langmuir 2007;23:387-90.

[18] Kang S, Lim S, Peck DH, Kim SK, Jung DH, Hong SH, et al. Stability and durability of PtRu catalysts supported on carbon nanofibers for direct methanol fuel cells. Int J Hydrogen Energy 2012;37:4685-93.

[19] Serp P, Corrias M, Klack P. Carbon nanotubes and nanofibers in catalysis. App Cat A: Gen 2003;253:337-58.

[20] Steigerwalt ES, Deluga GA, Lukehart CM. Pt-Ru/carbon fiber nanocomposites: synthesis, characterization, and performance as anode catalysts of direct methanol fuel cell. A search for exceptional performance. J Phys Chem B 2002;106:760-6.

[21] Girishkumar G, Hall TD, Vinodgopal K, Kamat PV. Single wall carbon nanotube supports for portable direct methanol fuel cells. J Phys Chem B 2006;110:107-14.

[22] Jiang Y, Wang X, Zhong L, Liu L. Design, fabrication and testing of a silicon-based air-breathing micro direct methanol fuel cell. J Micromech Microeng 2006;16:S233-9.

[23] Kelley SC, Deluga GA, Smyrl WH. A miniature methanol/air polymer electrolyte fuel cell. Electrohem and Solid-State Lett 2000;3(9):407-9.

[24] Kundu A, Jang JH, Lee HR, Kim SH, Gil JH, Jung CR, et al. MEMS-based micro-fuel processor for application in a cell phone. J Power Sources 2006;162:572-8.

[25] Santasalo-Aarnio A, Borghei M, Anoshkin IV, Nasibulin AG, Kauppinen EI, Ruiz V, Kallio T. Durability of different carbon nanomaterial supports with PtRu catalyst in a direct methanol fuel cell. Int J Hydrogen Energy 2012;37:3415-24.

[26] Rakov E G, Grishin D A, Garvilov Y V, Rakova E V, Nasibulin A G, Jiang H, et al. The morphology of pyrolytic carbon nanotubes with small number of walls. Russ J Phys Chem 2004;78 1966-71.

[27] Scotti G, Kanninen P, Mäkinen M, Kallio T, Franssila S. Silicon nanograss as micro fuel cell gas diffusion layer. Micro and Nano let 2010;5(6):382-5.

[28] Goswami S, Klaus S, Benziger J. Wetting and adsorption of water drops on Nafion films. Langmuir 2008;24:8627-33.

[29] Dresselhaous MS, Dresslhaus G, Saito R, Jorio A. Raman spectroscopy of carbon nanotubes. Phys Reports 2005;409:47-99.

[30] Behler K, Osswald S, Ye H, Dimovski S, Gogotsi Y. Effect of thermal treatment on the structure of multi-walled carbon nanotubes. J Nanopart Res 2006;8(5):615-25.

[31] Liu X, Suo C, Zhang Y, Wang X, Sun C, Li L, et al. Novel modification of Nafion 117 for a MEMS-based micro direct methanol fuel cell. J Micromech Microeng 2006;16:S226-32.

[32] Sabate N, Esquivel JP, Santander J, Torres N, Gracia I, Ivanov P, et al. Passive direct methanol fuel cells in silicon technology. J New Mat for Electrochem Sys 2008;11:143-6.

[33] Wozniak K, Johansson D, Bring M, Velasco A, Enoksson P. A micro direct methanol fuel cell demonstrator. J Micromech Microeng 2004;14:S59-63.

[34] Yen TJ, Fang N, Zhang X, Lu GQ, Wang CY. A micro methanol fuel cell operating at near room temperature. App Phys Lett 2003;83(19): 4056-8.

[35] Huang T, Liu J, Li R, Cai W, Yu A. A novel route for preparation of PtRuMe (Me = Fe, Co, Ni) and their catalytic performance for methanol electrooxidation. Electrochem Comm 2009;11:643-6.

[36] Kanninen P, Borghei M, Ruiz V, Kauppinen EI, Kallio T. The effect of nafion content in a graphitized carbon nanofiber-based anode for the direct methanol fuel cell. Int J Hydrogen Energy 2012;37:19082-91.

[37] Wang X, Li W, Chen Z, Waje M, Yan Y. Durability investigation of carbon nanotube as catalyst support for proton exchange membrane fuel cell. J Power Sources 2006;158:154-9.

[38] Ferreira PJ, La O' GJ, Shao-Horn Y, Morgan D, Makharia R, Kocha S, et al. Instability of Pt/C electrocatalysts in proton exchange membrane fuel cells. J Electrochem Soc 2005;152:A2256-71

[39] Frelink T, Visscher W, Veen JAR. Particle size effect of carbon-supported platinum catalysts for the electrooxidation of methanol. J Electroanal Chem 1995;382:65-72.

[40] Joo SH, Kwon K, You DJ, Pak C, Chang H, Kim JM. Preparation of high loading Pt nanoparticles on ordered mesoporous carbon with a controlled Pt size and its effect on oxygen reduction and methanol oxidation reactions. Electrochim Acta 2009;54:5746-53.

[41] Gan L, Du H, Li B, Kang F. The effect of particle size on the interaction of Pt catalyst particles with a carbon black support. New Car Mat 2010;25(1):53-9

[42] Y-Rintala E, Pasanen A, Kauranen P, Ruiz V, Borghei M, Kauppinen E, et al. Graphitic carbon nanofibers as catalyst support for PEMFC. Fuel Cells 2011;0:1-11.

[43] Park S, Lee JW, Popov BN. A review of gas diffusion layer in PEM fuel cells: Materials and designs. Int J Hydrogen Energy 2012;37:5850-65.

[44] Rakhshanpouri S, Rowshanzamir S, Water transport through PEM fuel cell in a seven-layer model. Energy 2013;50:220-231

[45] Gao Y, Sin GQ, Wang SL, Zhu S. Carbon naotubes based gas diffusion layers in direct methanol fuel cells. Energy 2010; 35:1455-9

[46] Carton JG, Lawlor V, Olabi AG, Hochenauer C, Zauner G. Water droplet accumulation and motion in PEM fuel cell mini-channels. Energy 2012;39:63-73.

[47] Mench MM, Wang CY. An In situ method for determination of current distribution in PEM fuel cells applied to a direct methanol fuel cell. J Electrochem Soc 2003;150(1):A79-85.

[48] Scotti G, Kanninen P, Kallio T, Franssila S. Integration of carbon felt gas diffusion layers in silicon micro fuel cell. J Micromech Microeng 2012;22:094006.